American Mineralogist, Volume 92, pages 1420–1427, 2007

Unique properties of lunar impact glass: Nanophase metallic Fe synthesis

YANG LIU,[1,*] LAWRENCE A. TAYLOR,[1] JAMES R. THOMPSON,[2,3] DARREN W. SCHNARE,[1] AND JAE-SUNG PARK[1,4]

[1]Planetary Geosciences Institute, Department of Earth and Planetary Sciences, University of Tennessee, Knoxville, Tennessee 37996, U.S.A.
[2]Department of Physics and Astronomy, University of Tennessee, Knoxville, Tennessee 37996, U.S.A.
[3]Oak Ridge National Lab, Oak Ridge, Tenneessee 37831, U.S.A.
[4]Department of Mechanical, Aerospace, and Biomedical Engineering, University of Tennessee, Knoxville, Tennessee 37996, U.S.A.

ABSTRACT

Lunar regolith contains important materials that can be used for in-situ resource utilization (ISRU) on the Moon, thereby providing for substantial economic savings for development of a manned base. However, virtually all activities on the Moon will be affected by the deleterious effects of the adhering, abrasive, and pervasive nature of lunar dust (<20 μm portion of regolith, which constitutes ~20 wt% of the soil). In addition, the major impact-produced glass in the lunar soil, especially agglutinitic glass (60–80 vol% of the dust), contains unique nanometer-sized metallic Fe (np-Fe^0), which may pose severe pulmonary problems for humans.

The presence of the np-Fe^0 imparts considerable magnetic susceptibility to the fine portion of the lunar soil, and dust mitigation techniques can be designed using these magnetic properties. The limited availability of Apollo lunar soils for ISRU research has made it necessary to produce materials that simulate this unique np-Fe^0 property, for testing different dust mitigation methods using electromagnetic fields, and for toxicity studies of human respiratory and pulmonary systems, and for microwave treatment of lunar soil to produce paved roads, etc. A method for synthesizing np-Fe^0 in an amorphous silica matrix is presented here. This type of specific simulant can be used as an additive to other existing lunar soil simulants.

Keywords: Nanophase Fe, metallic Fe, lunar dust, ferromagnet, microwave coupling, magnetization

INTRODUCTION

The recent initiative in human space exploration involves settling the Moon, producing rocket propellants, and establishing the Moon as a test bed in preparation for future missions to Mars and beyond. The surface of the Moon is covered by a layer of lunar regolith, which can provide important materials for in-situ resource utilization (ISRU). Structurally bonded oxygen and solar-wind implanted hydrogen in lunar soil can be readily released from glass and minerals to be used as propellants, as well as for making water for human consumption (e.g., Taylor 1992). However, lunar dust (the <20 μm portion of the regolith) presented several unanticipated problems during the Apollo missions (Taylor et al. 2005). With plans for returning humans to the Moon, it is paramount that dust mitigation studies be undertaken immediately. The results of this present study provide for a critical component that allows testing of various dust mitigation methods.

Dust comprises ~20 wt% of lunar soil (McKay et al. 1991). The adhesive, abrasive, and omnipresent lunar dust is involved with virtually every aspect of the planned human presence on the Moon. For example, an embarrassing problem for the Apollo program involved the fact that none of the "million-dollar rock boxes" designed and built at Oak Ridge National Labs remained sealed at the vacuum of the Moon (~10^{-12} torr). They all leaked, because of the ubiquitous dust, thereby exposing the lunar samples to terrestrial air. The deleterious nature of lunar dust became apparent with the first Apollo mission to the Moon, but was tolerated rather than mitigated because of the rapid succession of following missions. Without any effective mitigation, large amounts of lunar soil and dust were brought into the lunar module, thereby contaminating the atmosphere that the Apollo astronauts breathed. In fact, each astronaut complained of some form of irritation to their noses, throats, and/or eyes (Taylor et al. 2005). It is entirely possible that the large proportions of the <1 μm fraction of lunar dust (~1 wt% of lunar soil) may have real potential for being toxic to humans, forming various pulmonary fibroses, etc. Lunar dust is composed of 60–80 vol% impact-produced glass (agglutinitic glass, Fig. 1), which contains abundant nanometer-sized metallic Fe grains (np-Fe^0; Taylor et al. 2005). Glass particles of <100 nm can move directly into the human blood stream, and we suspect that the highly reducing metallic Fe may interact with hemoglobin Fe^{3+}, causing reduction to Fe^{2+}, severely affecting the oxidation state of the respiratory system. Furthermore, Park et al. (2007) have determined that the particle size distribution (PSD) of lunar dust from Apollo 11 soil has a peak at ~100 nm, indicative of a huge number of dust particles in this dangerous size range.

* E-mail: yangl@utk.edu

0003-004X/07/0809–1420$05.00/DOI: 10.2138/am.2007.2333

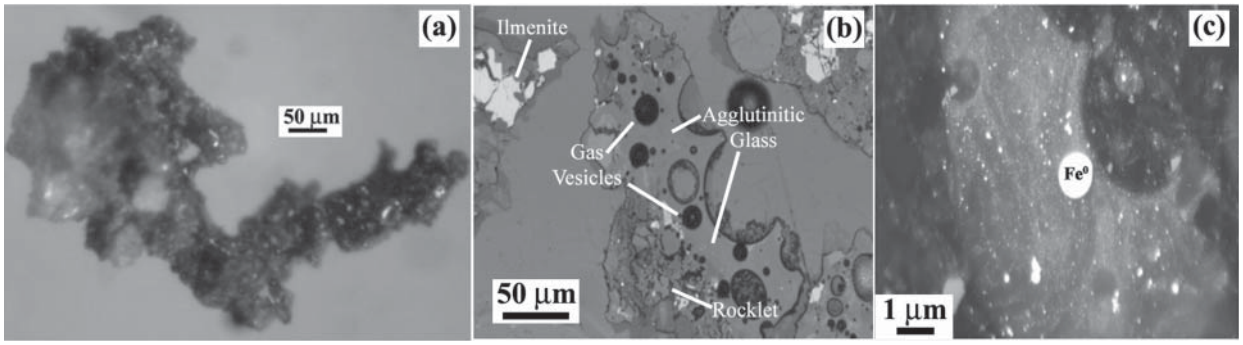

FIGURE 1. Lunar agglutinates. (**a**) Optical image of an agglutinate grain in Apollo 17 soil 70051. (**b**) Agglutinate grain sectioned and viewed optically in reflected light (courtesy of Dave McKay). (**c**) Back-scattered electron (BSE) image of an agglutinate shows a "milky way" of nanometer-sized metallic Fe grains (white spots) (courtesy of Dave McKay). Both **b** and **c** show high abundances of vesicles; these probably formed when solar-wind-implanted volatiles escaped during impact-melting of the soil to produce the cement that binds the lithic, mineral, and glass particles together to form the agglutinate.

Mitigation methods need to be designed to minimize the various aspects of potential lunar dust problems. Fortunately, these unique np-Fe^0 grains also impart a distinct magnetic susceptibility to the lunar soil. Almost all lunar dust (<20 μm) is attracted by a hand magnet because of this metallic np-Fe^0 (Taylor et al. 2005). Most soil fragments have a vapor-deposited glass coating containing suspended np-Fe^0 particles (Keller and McKay 1997; Wentworth et al. 1999). In addition, these abundant np-Fe^0 particles cause exceptional interaction (i.e., coupling) of lunar soil with 2.45 GHz microwaves in a normal kitchen oven, such that "lunar soil will melt at 1200 °C, before your tea-water will boil," a discovery made recently by Taylor and Meek (2004, 2005). These characteristics have important bearings on dust mitigation on the Moon. For example, a simple magnetic filter can remove >90% of all lunar dust from air; a microwave machine can effectively pave portions of the lunar surface, making "dust-less landing pads" and roads (Taylor and Meek 2004, 2005).

The U.S. Apollo and Soviet Luna Missions collected ~382 kg of rocks and soils. However, these are too precious to use for most ISRU projects; therefore, it is imperative that suitable lunar soil simulants be made for numerous science/engineering purposes. For example, various tests on dust-mitigation methods and studies of physiological effects require large amounts of materials with np-Fe^0. Thus, similar materials synthesized to contain np-Fe^0 are needed for these tests.

Three experimental methods have been reported for the production of np-Fe^0, with respect to the space-weathering formation of lunar regolith. The first method, an impregnation method, was developed by Morris et al. (1989) for simulating space weathering on Mars and then adapted by Allen et al. (1996) and Noble et al. (2003) to produce np-Fe^0. Commercially purchased silica gels with nanometer-sized pores (2–30 nm) were submerged in Fe^{3+} nitrate solution with different concentrations. Then the impregnated gel was heated at 550 °C to produce nanometer-sized hematite particles. Data in Table 1 in Morris et al. (1989) fall in a linear trend with a slope of 1 wt% Fe_2O_3/cycle, where a cycle includes impregnation and heating at 550 °C. Therefore, to obtain ~10 wt% Fe_2O_3, the impregnation and heating needed to be repeated ~10 times. Allen et al. (1996) and Noble et al. (2003) reduced the Fe_2O_3-loaded gel at 850–900 °C with flowing H_2 to produce np-Fe^0 particles in the silica matrix. This method is suitable for production of glass with np-Fe^0, but it is limited to a binary composition (i.e., SiO_2-Fe^0), as the matrix is only SiO_2, and the exact amount of Fe added is difficult to control (Noble et al. 2003). The second method is by direct reduction of silicate glass and minerals (Allen et al. 1993). However, the size of the Fe grains (up to 1 μm) is much bigger that in typical lunar agglutinitic glass (~3–50 nm). The third method involves laser irradiation of minerals (Yamada et al. 1999; Sasaki et al. 2001). Pellets of olivine and pyroxene are irradiated with a pulsed (6–8 ns) laser beam under vacuum. After multiple irradiations, a thin glass rim with nanometer-sized Fe particles can be observed on the surface of the minerals. This method is inefficient and cannot control the amount of Fe produced. It would be virtually impossible to produce usable amounts of simulant (e.g., 1–10 g) using the irradiation method. Here, we report a unique method for synthesizing np-Fe^0 in an amorphous silica-rich glass matrix. Preliminary results on a method for making Fe^0 grains in multi-component glass matrix, much akin in composition to lunar impact-generated agglutinitic glasses, are also reported.

EXPERIMENTAL AND ANALYTICAL METHODS

We have developed a new method that can synthesize nanometer-sized metallic Fe in amorphous silicate glasses with varying compositions. Here we present methods for both two-component (SiO_2-FeO, hereafter referred to as SF) and five-component (SiO_2-Al_2O_3-MgO-CaO-FeO, hereafter referred to as SAMCF) products.

The method for synthesizing binary samples was adapted from the method in the literature for synthesizing Fe^{3+}-doped, silica-gel glass (e.g., Ennas et al. 1998; Morris et al. 1999). However, the time taken to form the gel is long (up to several days) if silicon tetraethoxide [TEOS, $Si(OC_2H_5)_4$] is used as the precursor of SiO_2. Instead, we used a solution of pre-condensed silica (Silbond H-5) as suggested on the website of the Microstructured Materials Group at Lawrence Berkeley National Laboratory (http://eande.lbl.gov/ECS/aerogels/satoc.htm). Silbond H-5 was mixed with an equal volume of ethanol solution (70 vol% EtOH) in a 500 mL beaker and the solution was stirred magnetically for 30 min. A catalyst solution, prepared by mixing ethanol, distilled water, and 30% NH_4OH (volume ratio 1:1.2:0.007) was added slowly into the Silbond and ethanol solution. The transparent liquid became viscous in 20–30 min after adding the catalyst solution. At this time, an Fe-nitrate solution (pH = ~2, adjusted using 0.1 *M* NH_4OH) was stirred into the viscous liquid to form a homogeneous mixture with a reddish-brown color from Fe^{3+} ions. The beaker was then covered and kept at room temperature for 2–3 days to ensure that Fe^{3+} ions were distributed uniformly in the mixture, and the gel had sufficient time to form an SiO_2 framework. After such aging time, the mixture was dried slowly

at 65–100 °C on a hot plate over a period of about 2 days. At the end of this heating step, orange to brown pieces of dried gel (<1 cm in size) were produced. The sample was further dried at ~100 °C. The fragments shrank to a few millimeters in size. Emphasis was not placed on maintaining any particular shape of the gel, since our goal was to make a soil-like material. The red-brown fragments were then heated, in flowing nitrogen, in a horizontal tube furnace at 350–400 °C for >10 h to further dry the sample, decompose the NO_3^-, and remove the resulting NO_2. The color of the amorphous materials changed to blackish brown. SF samples with target compositions of ~90 wt% SiO_2 and ~10 wt% FeO (named as SF10), ~80 wt% SiO_2 and ~20 wt% FeO (named as SF20), and ~60 wt% SiO_2 and ~40 wt% FeO (named as SF40) were prepared using this method.

For the five-component system, a target composition of ~53 wt% SiO_2, ~14 wt% Al_2O_3, ~11 wt% MgO, ~11 wt% CaO and ~11 wt% FeO was used to simulate the lunar agglutinitic glass (Taylor et al. 2001). Both TEOS and Silbond H-5 were used as the starting material for SiO_2. The starting materials for other oxide components included Al nitrate [$Al(NO_3)_3{\cdot}9H_2O$], Ca nitrate [$Ca(NO_3)_2{\cdot}4H_2O$], Mg nitrate [$Mg(NO_3)_2{\cdot}6H_2O$], and Fe nitrate [$Fe(NO_3)_3{\cdot}9H_2O$]. If TEOS was used, TEOS, 100% EtOH, and distilled water were mixed in a volume ratio of 1:1:0.5. This solution was stirred for 30 min to ensure complete hydrolysis of TEOS. Then, a hydrous solution of all nitrates was slowly added to the TEOS solution. After stirring for 1 h, the mixture was kept in a warm-water bath at ~60 °C to evaporate water and ethanol. The gelation time depends on the amount of water in the solution and can range from 3 to more than 6 h. When the mixture lost its fluidity, the container was covered and kept at room temperature for 2–3 days. We also tested Silbond H-5 as the source for SiO_2. Equal volumes of Silbond H-5 and ethanol were mixed and stirred for 30 min, and the catalyst solution was added slowly. When the mixture became viscous, a hydrous solution of nitrates was added. The mixture was kept at 45–60 °C to evaporate water and ethanol. Once the mixture became a solid gel, the container was covered and stored at room temperature for two days. At the end, the solid gel was dried on a hot plate from 60 to 100 °C over a period of 1–2 days. During drying, the gel cracked and crumbled. Then, the fragments were heated in nitrogen flow through a horizontal tube furnace at ~350 °C, to drive off NO_2. Powder X-ray diffraction (XRD) was performed on several of the SF and SAMCF samples after the ~350 °C heating, using a Siemens D500 X-Ray diffractometer at the University of Tennessee.

To generate metallic Fe, samples were reduced multiple times under flowing pure H_2 in a horizontal tube furnace, at high temperatures. Different temperatures and durations were tested. At the early stage of our experiments, a large tube furnace was used because it could hold a large amount of sample (up to 30 g). The inner diameter of the ceramic tube was 45 mm. The sample was loaded in a glass boat (5 cm long, 3.8 cm wide, and 2 cm deep) and heated for 3–5 h at 700–880 °C. Because of the complex composition of the SAMCF samples, they were reduced at ~750 °C to avoid significant crystallization of silicates. These samples were reduced for ~4 h under flowing H_2. At the end of the reduction experiments, the furnace was switched off and cooled slowly under H_2 flow to 700 °C. Then, the H_2 flow was discontinued, and samples were cooled slowly under N_2 flow. All but one SF10 sample, SF40, and all SAMCF samples were reduced using the large-tube furnace. After each reduction, XRD spectra of samples were collected. If the metallic Fe diffraction peak was small, samples were ground and reduced again. To further study the kinetics of the reduction process, a detailed set of experiments was conducted on one sample (1.4 g of SF10-4).

A smaller furnace with a quartz tube (~25 mm in diameter) was used for SF10-1 and all SF20 samples. Samples (up to 10 g) were placed in a silica-glass boat (7 cm long, 2 cm wide, and ~1.5 cm deep), which was positioned in the furnace so that its center was at the hot spot. The temperature gradient along the boat was small (<10 °C). Experimental temperatures ranged from 770 to 1000 °C. After 1–2 h of reduction, samples were cooled under N_2 flow, reground, and reduced again. Each SF20 (20 wt% FeO) sample was processed in this manner for 3–5 times. Samples were cooled rapidly in 1–2 h by cooling the tube in air while the sample was bathed in N_2. The reduced sample has a black color and is readily attracted by a hand magnet. Powder XRD was performed on all reduced samples. Experimental conditions of several samples are listed in Table 1.

Several of the finished samples (SF10-1, SF10-3, SF10-4, and SAMCF-2) were fused on a Mo-strip in N_2 atmosphere to form a fused sample of the powder. Grains of some other reduced samples (especially SAMCF samples) were embedded in epoxy. These grains and fused beads of SF and SAMCF samples were polished and analyzed using a Cameca SX50 electron microprobe (EMP) at the University of Tennessee to test homogeneity and to obtain a bulk composition. The analytical conditions include a beam of a 10–15 µm diameter at 15 kV and 10 nA beam current. Back-scattered-electron (BSE) images were also collected on the polished grains with a JEOL 6060LV Scanning Electron Microscope. Fine powders used for XRD were also imaged using a Hitachi H-800 TEM at the University of Tennessee to determine the size of the metallic Fe^0. The magnetic properties of two SF10 samples, one SAMCF sample, an Apollo soil (70051), and a lunar soil simulant (JSC-1Af) were measured using a Quantum Design MPMS-7 SQUID-based magnetometer at the Oak Ridge National Laboratory. The approximate metallic Fe contents in the lunar sample and our synthetic samples were determined from the magnetic measurements (see discussion below).

TABLE 1. Experimental conditions for selected samples

Sample	Starting material	*T* (°C) *	Duration (h)	Crystalline phases†
SF10-1	Silbond H-5	880	4	Fe, ol
SF10-3	Silbond H-5	720–750	3	Fe, qtz, ol
		600	3	
		910	2	
SF10-4	Silbond H-5	870	2	Fe, ol
SF20-1	Silbond H-5	930	1	Fe, qtz, ol
		970	1	
		910	1.5	
		970	1.5	
SF20-6	Silbond H-5	810	1.3	Fe, ol
		940	1.7	
		810	1.5	
		810	2	
		850	1	
SF20-12	Silbond H-5	840	1.5	Fe, qtz, ol
		930	2	
		890	1.5	
		850	17	
SF40	Silbond H-5	860	4	Fe, qtz, ol
		870	4	
SAMCF-1	Silbond H-5	705	3	Fe, ol
SAMCF-2	TEOS	705	2	Fe, ol
		715	3	
SAMCF-10	TEOS	700	3	Fe, ol
SF10-4a‡	first	870	2	Fe, ol
	2nd	865	4	
	3rd	865	5	
	4th	870	3.5	Fe, ol
	5th	850	3	Fe, ol
	6th	860	3	Fe, ol

* Temperature variations in experiments were usually ~20 °C.
† ol indicates olivine, qtz indicates quartz.
‡ SF10-4a is part of SF10-4 (1.4 g) that was used to study reduction rates. Between each heating, the sample was ground to breakup the annealed silica matrix.

RESULTS AND DISCUSSION

Characteristics of samples

Metallic Fe particles in binary samples are distributed uniformly (Figs. 2a and 2b). Most Fe particles are ~30 nm in SF10 samples, ~60–70 nm in SF20 samples, and ~80–100 nm in SF40 samples. However, for each sample, a range in grain size is observed. The range of the particle size could be caused by inhomogeneous drying/evaporation of interstitial water and ethanol in the gel. The important point is that the size of virtually all Fe grains in SF10 samples and significant proportion (>35%) of Fe grains in SF20 and SF40 samples are nanophase (<100 nm). Some less opaque grains may be mainly fayalite. However, the resolution of the TEM is not sufficient to distinguish this. The

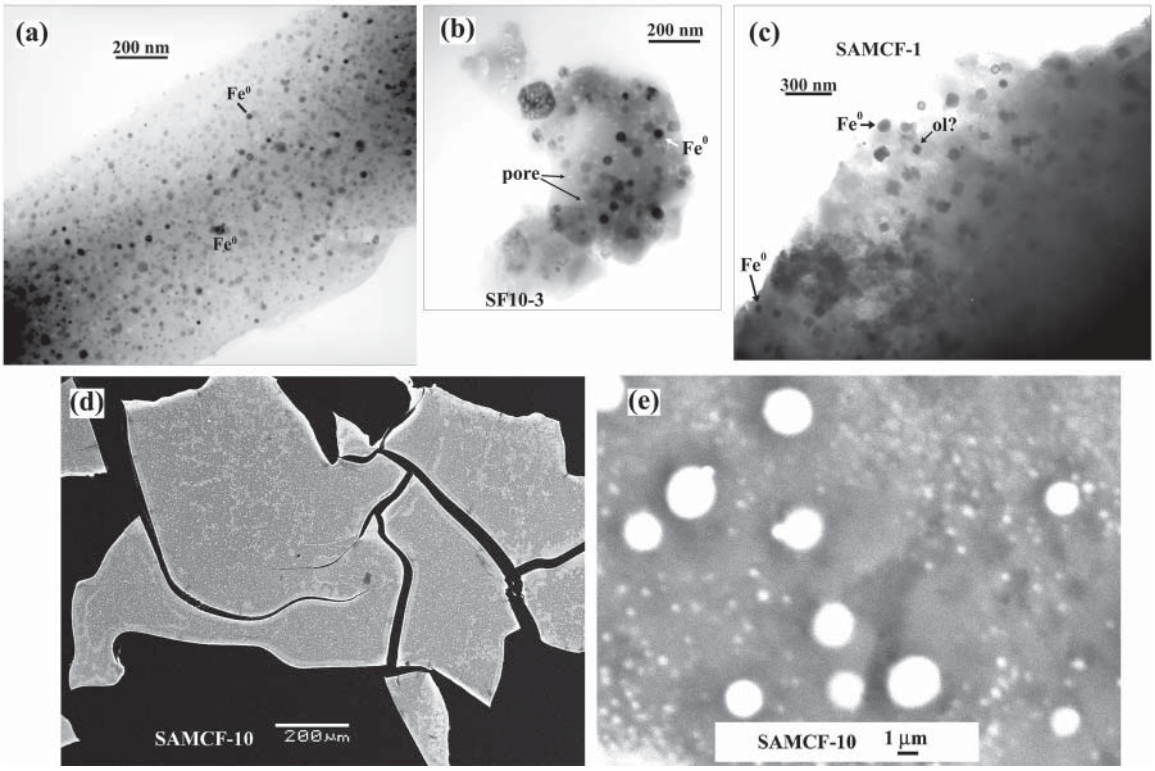

FIGURE 2. TEM and SEM images of synthetic samples. (**a**–**c**) are bright-field TEM images. (**a** and **b**) SF10 samples on the same scale. These two SF10 samples have uniform distributions of np-Fe^0 particles. Sample SF10-3 contains slightly larger np-Fe^0 grains than SF10-1. (**c**) The SAMCF-1 sample with slightly different scale. Euhedral grains may be olivine crystals. (**d** and **e**) BSE images of SAMCF-10 grains. Bright spheres are metallic Fe. The sample is heterogeneous with a Ca-rich rim near edges and crack surfaces.

samples also contain nanopores that are slightly smaller than the np-Fe^0. TEM and SEM images of SAMCF samples (Figs. 2c–2e) show that Fe particles (up to 2 μm) are larger than those in the binary samples. The larger Fe grain sizes in SF20, SF40, and five-component samples may be a result of a more open framework with the lower SiO_2 content.

After H reduction, all samples contained amorphous silicate, metallic Fe (α-Fe^0), and fayalite (Fe^{2+}; Fe_2SiO_4), and occasional quartz, as shown by the XRD spectra (Table 1, Fig. 3). The oxygen fugacity of the experiments was near $\log f_{O_2} \approx -19$ at >900 °C using the reaction of $Fe_2SiO_4 = SiO_2 + 2Fe + O_2$ (Shi 1992). All binary and five-component samples contained olivine (fayalite for binary samples). We know that olivine was produced only during hydrogen reduction because samples only contained hematite after the initial decomposition of the nitrate gel mixture at 350 °C. The presence of Fe^{2+} may be the result of intrinsic oxygen fugacity. Alternatively, Fe^{2+} is shielded from reaction with H_2 because of the consolidation of the surrounding silicate at high temperature. As an example, the SF20-12 sample was heated at 870 °C in pure H_2 atmosphere for ~17 h, but the XRD spectrum shows that the sample still contains fayalite (Fig. 3a). However, the SF10-4 sample that was reduced repeatedly with grinding shows increasing Fe^0 content (Fig. 3b). Metastable quartz was produced at $T > 900$ °C or after a long-duration experiment at 870 °C. The SF20 samples reduced at 870 °C for a short period contain no detectable quartz (e.g., SF20-6 in Fig. 3a). The SF40 sample which it was reduced at 870 °C for only 8 h does contains quartz. There appears to be a tradeoff between Fe^0 and quartz contents. Samples with higher quartz content also contain relatively higher Fe^0 than samples without quartz as shown by the intensity of the most intense XRD peaks (Fig. 3a).

The compositions of SF10 and SF20 samples, as determined with the EMP, are similar to the target composition (Table 2), suggesting the efficient entrapment of Fe^{3+} in the silicate structure during gelation and drying. The SF40 sample contains less FeO than the target content, which reflects loss of FeO during gelation and drying. The SAMCF samples also contain lower oxide concentrations than the target composition, especially for CaO and MgO. Because the SF40 and SAMCF samples contain low SiO_2 contents, the framework of SiO_2 in the gel is considerably open and thus cannot efficiently trap the cations during gelation.

The EMP results have large standard deviations, representing elemental heterogeneity. For fused beads of SF10-1, SF10-3, and SF10-4, the large deviations are partially a result of the insufficient mixing between metallic Fe and high viscosity SiO_2 during Mo-strip heater melting. However, large standard deviations for SAMCF-2 and for grain mounts of SF20 and SF40 suggest that these samples are heterogeneous. Grains of SF20-1 and SF40 samples show different brightness in BSE images. SEM images of polished SAMCF grains show that these samples contain bright rims near original surfaces and along cracks (e.g., Fig. 2d), which contain higher CaO (16 wt%) than the dark regions

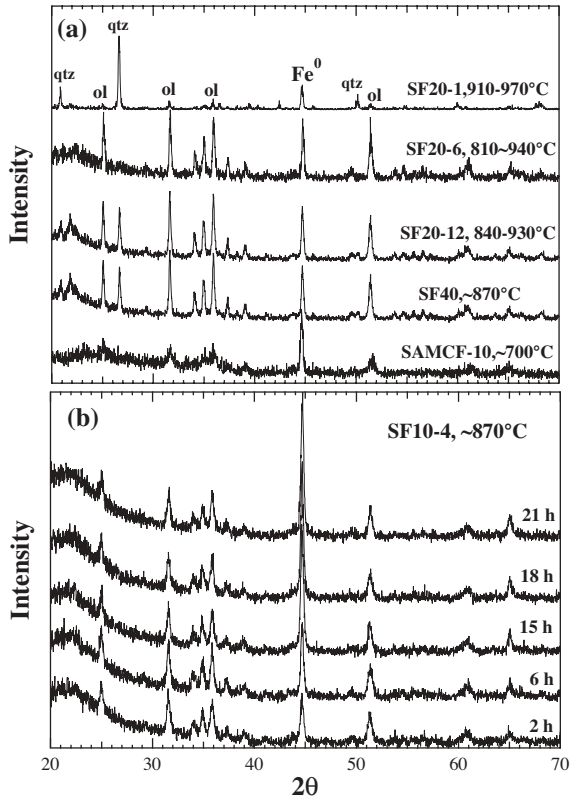

FIGURE 3. XRD patterns of reduced samples using Cu*K*α radiation (patterns are offset for clarity). (**a**) XRD patterns of SF20, SF40, and SAMCF-1 samples. Olivine peaks are labeled as ol, and quartz peaks are labeled as qtz. The broad peak centered at 2θ ≈ 22° corresponds to the amorphous glass. See Table 1 for details. (**b**) XRD spectra of SF10-4 sample that went through repeated reductions. Between each heating, the sample was ground to enhance the permeability. The accumulative duration is shown for each curve. Note the increasing intensity of Fe^0 peak with incremental heating.

(~4–5 wt% CaO). The heterogeneity in the samples is possibly due to a non-uniform temperature distribution, caused by drying on the hot plate.

In summary, the best temperature for reduction appears to be 850–870 °C for binary samples with 10–20 wt% FeO. The reduction temperature should be lower for samples with higher FeO content. Short annealing periods and several grindings aid in obtaining high metallic Fe contents. Different drying mechanisms, such as supercritical drying or more-uniform drying at low temperatures (~65 °C) using a container with a larger surface area, should increase homogeneity. For five-component samples, melting at high temperature under mixed H_2 and N_2 atmosphere can improve the homogeneity, albeit at a slight increase in metallic Fe grain size, due to ripening.

Magnetic properties and metallic Fe content

Measurements of the magnetization (*M*) were performed in magnetic fields (*H*) up to 15 000 Oe (1.5 Telsa) at –268 °C (5 K) and 17 °C (290 K). Figure 4a shows examples of *M* vs. *H* for several major types of magnetic materials (Dunlop and Özdemir1997; Butler 1992). Placing a material in a magnetic field (H) induces a macroscopic magnetic moment (*m*) when its atomic dipoles, either individually or collectively, try to align with the external field. The *M*-*H* curves of ferro/ferri-magnetic (FM) materials are clearly different from other types of magnetic materials (Dunlop and Özdemir 1997; Butler 1992). Iron, nickel, and cobalt are ferromagnetic elements, and titanomagnetite is a typical ferromagnetic material. FM materials tend to keep a memory of the field and form an open, irreversible hysteresis loop. The size of the loop is basically defined by several parameters: saturation magnetization (M_s), remanence (M_r), and coercivity (H_c). The saturation magnetization is independent of grain size, but is proportional to the concentration of FM materials in the sample. When particle size decreases below a critical value, the FM materials become super-paramagnetic (SPM), leading to an S-shaped curve that goes through the origin (M_r = 0). When there is a mixture of SPM and PM materials, the hysteresis loop becomes narrower. Diamagnetism (DM) occurs in all materials, but its signal is often overwhelmed by other types of magnetic response and/or signals from other phases. Typical DM materials are silica, calcite, and water. Paramagnetic (PM) materials include less polymerized silicates (e.g., biotite, fayalite). Pure olivine, ulvöspinel, and ilmenite form a category of anti-ferromagnetic (AFM) materials. They have a PM response at temperatures above a critical value (Néel Temperature), which are –153 °C and about –233 °C for ulvöspinel and ilmenite, respectively. At –268 °C (5 K), the magnetization curves for PM, AFM, and SPM will change. In large magnetic fields, PM materials at 5 K have S-shaped curves similar to those of SPM at room temperature. Also, 5 K is below the Néel

TABLE 2. Compositions of samples

	SF10-3		SF10-4		SF20-1		SF40			SAMCF-2	
Oxides	target*	EMPA†	target*	EMPA†	target*	EMPA†	target*	EMPA†		target*	EMPA†
SiO_2	89	88 (4)	87	88 (5)	80	82 (8)	60	61(4)	SiO_2	55	66 (3)
FeO^T ‡	11	11 (4)	13	12 (5)	20	19 (8)	40	34(5)	Al_2O_3	10	7.1(6)
Total		99		100		101		94	MgO	12	8.0 (6)
Fe^0 §		2.3		1.8		n.a.			CaO	15	10.8 (7)
		N = 120		N = 78		N = 72		N = 32	FeO^T	8	7.7 (7)
									Total		99.2
											N= 30
									Fe^0 ‡		1.3

Notes: N is the total number of analyses. Numbers in parentheses are the standard deviation of N analyses as expresses in terms of the last significant digit. Total of the EMPA analyses is the average original total.

* Target composition is calculated from starting materials used in preparation.

† Electron microprobe analyses (EMPA) were conducted on fused beads of SF10-3, SF10-4, SAMCF-2 and on individual grains of SF20-1 and SF40.

‡ FeO^T is the total Fe including both FeO and Fe expressed as FeO.

§ Fe^0 is calculated from the saturation magnetization obtained from the magnetic measurements (Table 3). n.a. indicates that Fe^0 was not analyzed.

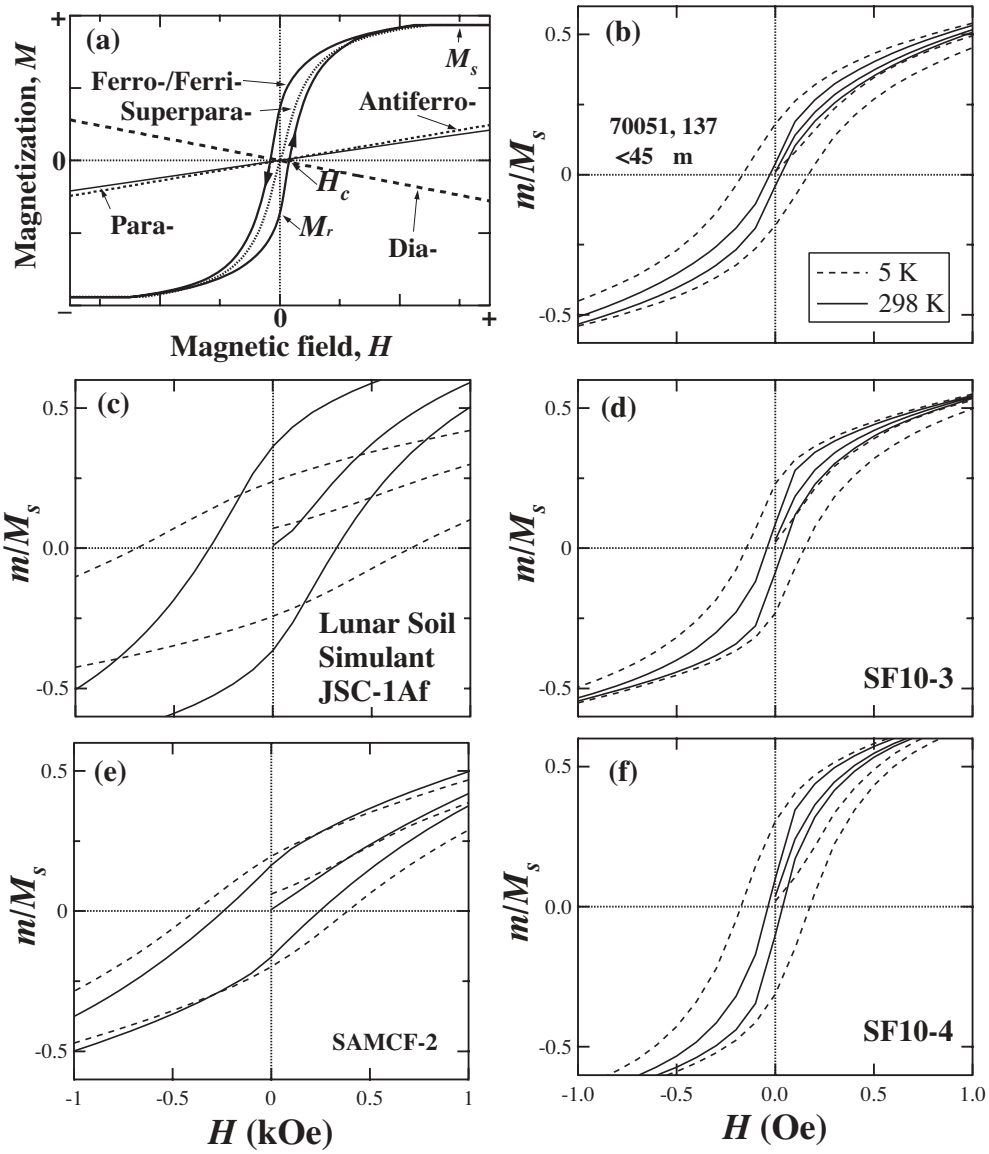

FIGURE 4. Magnetization curves of various samples. (**a**) Responses of different magnetic materials. Here magnetization *M* is magnetic moment (*m*) divided by mass. M_s and M_r represent the saturation and the remanent magnetization, respectively. H_c is coercivity. See text for details. (**b**) Magnetization curve for Apollo 17 soil 70051. (**c**) Lunar soil simulant (JSC-1Af), made from a terrestrial volcanic tuff. (**d**) Synthetic material (SF10-3). (**e**) Synthetic material (SAMF-2). (**f**) Synthetic material (SF10-4). For **b–f**, the paramagnetic signals were subtracted. M_s for **b–f** were obtained at $H > 11$ kOe (outside the plot area).

temperature for many AFM materials (pure ilmenite), where they only exhibit a small magnetization that increases linearly with *H*. However, at this temperature, SPM will start to show hysteresis. To a first approximation, the wider hysteresis loop at –268 °C (5 K) for the same sample indicates that the sample contains SPM materials.

Magnetization curves of FM materials in the lunar soil (Fig. 4b), lunar soil simulant JSC-1Af (Fig. 4c), SF10 samples (Figs. 4d and 4f), and SAMCF-2 sample (Fig. 4e) were plotted by subtracting out the linear, paramagnetic signal due to the matrix. The simulant JSC-1Af is the fine portion (<20 µm) of lunar soil simulant JSC-1A, which is a clone of a former simulant JSC-1. To simulate the geotechnical properties of lunar soil, JSC-1 was produced in 1993 by crushing a basaltic tuff (McKay et al. 1994). JSC-1A contains ~0.4 wt% Ti-magnetite (Hill et al. 2007). For FM particles below a critical grain size, the magnetic response becomes super-paramagnetic (SPM), meaning that the *M*-*H* curve becomes reversible. Nanophase Fe becomes SPM near room temperature for grains in the range 8–26 nm (Dunlop and Özdemir1997). Our results are consistent with these suggested critical values. The hysteresis loop of the Apollo 17 soil 70051 (Fig. 4b) and synthetic SF10-3 (Fig. 4d) and SF10-4 (Figs. 4d and 4f) are very narrow at 290 K. Upon decreasing temperature, the hysteresis loop of these three samples opened up by a factor

TABLE 3. Parameters defining the hysteresis loop

Sample	Weight (mg)	$M_{s,290K}$* emu/g	$M_{r,290K}$* emu/g	$H_{c,290K}$ (Oe)	$\chi_{0,290K}$* 10^{-5} emu/g/Oe	$\chi_{pm,290K}$* 10^{-5} emu/g/Oe	FM† wt%	A_{loop}‡ 10^{-5}J/g/cycle	$M_{s,5K}$ emu/g	$M_{r,5K}$ emu/g	$H_{c,5K}$ (Oe)	$\frac{H_{c,5K}}{H_{c,290K}}$	$\frac{M_r/M_{s,5K}}{M_r/M_{s,290K}}$
SF10-3	59	5.090	0.436	42	1123	0.6064	2.31	5.70	5.361	1.231	154	3.7	2.7
SF10-4	58	3.993	0.398	37	1034	0.7986	1.81	4.98	4.139	1.260	174	4.7	3.1
SAMCF-2	61	2.866	0.469	242	148	1.59	1.30	17.9	3.393	0.670	351.8	1.5	1.2
70051	50	1.705	0.067	27	280	1.024	0.77	3.15	2.883	0.521	152	5.6	4.6
JSC-1Af	65	0.591	0.215	313	32	0.7820	0.91	8.43	1.229	0.293	439	1.4	0.6

* Saturation magnetization M_s, remanent magnetization M_r, and observed initial magnetic susceptibility χ_0 are based on magnetic moment (in emu = erg/G) divided by sample weight.
† The fraction of ferro-/ferri-magnetic materials in the sample. It can be estimated using Ms_{290K} and the mass magnetization of the bulk materials. For Apollo 17 soil 70051, synthetic SF10-3 and SF10-4, the content of Fe^0 was calculated using a mass magnetization of 220 emu/g at 290 K for bulk Fe. For the simulant JSC-1Af, the content of Ti-magnetite was estimated using a mass magnetization of 90 emu/g for bulk Ti-magnetite.
‡ Area of the hysteresis loop for a maximum H of 15 000 Oersted was divided by sample weight. This area corresponds to the maximum possible work per cycle that can be done by an alternating magnetic field, thereby generating heat.

of 2.7–4.6 for the ratio of magnetizations M_r/M_s and a factor of 3.7–5.6 for the coercive field H_c (Table 3). In addition to the TEM evidence presented in Figure 2, this finding also demonstrates that most of the Fe grains in the SF samples are in the diameter range of 10–30 nm. The smaller increments of M_r/M_s and H_c upon decreasing temperature (1.2 and 1.5, respectively) for SAMCF-2 sample reflect the larger Fe^0 grain sizes. Ti-magnetite in JSC-1Af contributed to its magnetic signal (Fig. 4c), the majority of which are above the critical size for SPM behavior (80 nm, Dunlop and Özdemir1997).

The saturation magnetization at 17 °C (Table 3) was used to derive the contents of FM materials in the sample (Fe^0 in synthetic SF10-3, SF10-4, and SAMCF-2; mostly Fe^0 in the <45 μm fraction of Apollo sample 70051, Ti-magnetite in JSC-1Af, Table 3). The metallic Fe in SF10 and SAMCF samples comprises only ~1/5 of the total FeO available. As discussed above, the annealing of silicate matrix and intrinsic O may result in the incomplete reduction. Experiments at higher H_2 or $H_2 + N_2$ pressure may help to increase the metallic Fe^0 content. Synthetic samples SF10-3 and SF10-4 contain 1 to 1.5 wt% more Fe^0 than Apollo 17 soil 70051 (0.77 wt%). At room temperature, the M_r/M_s ratios and H_c of synthetic SF10-3 and SF10-4 overlap at the upper end of all lunar rocks and soils, whereas those for SAMCF-2 are outside the range of lunar rocks and soils (Fig. 5). The initial mass susceptibilities (χ_0) of Apollo 17 soil 70051 and synthetic samples SF10-3, SF10-4, and SAMCF-2 at 290 K are much larger than JSC-1Af, reflecting different FM materials in the sample (metallic Fe for lunar soil and the synthetic samples) and especially the large magnetic irreversibility of the JSC-1Af material with a coercive field H_c >300 Oe, nearly an order of magnitude larger than the samples containing Fe in nanoparticle form. Microwave melting experiments were conducted on a mixture of our SF10-4 simulant and JSC-1A (Hill and Taylor 2006). Results show that addition of our SF10-4 simulant increases considerably its ability to couple with microwaves and decreases the reaction times of JSC-1A with microwaves (E. Hill, pers. comm.), which can be attributed largely to the higher electrical conductivity of metallic Fe (in SF10 simulants), compared with Ti-magnetite.

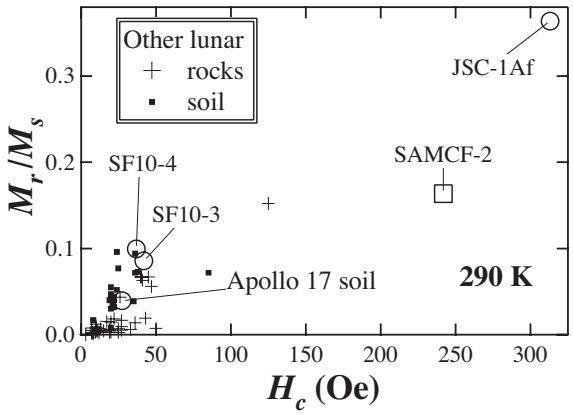

FIGURE 5. Parameters defining the hysteresis loop (M_r, M_s, and H_c, see Fig. 4a) are plotted for comparison of the different samples. Data for other lunar rocks and soils are from Brecher et al. (1974); Nagata et al. (1970, 1972, 1973, 1974); Pearce et al. (1973, 1974); and Pearce and Chou (1977).

SUMMARY REMARKS

The nanophase metallic Fe in lunar soil, the direct result of space weathering during soil formation, imparts magnetic properties to the soil, which have many potential applications for dust mitigation on the Moon. Nanophase Fe in amorphous silica was successfully synthesized using the method reported in this paper. The nanophase Fe, dispersed homogeneously in the amorphous silica, is similar to that in lunar soil in terms of grain size and magnetic properties. When mixed with lunar soil simulant JSC-1Af, extreme coupling of this nanophase Fe additive with 2.45 GHz microwave energy provides for numerous dust-mitigation possibilities (e.g., landing pads, paved roads, habitats, oxygen production, etc.). We recommend this silicate glass with suspended nanophase Fe as an additive to lunar regolith simulant for the performance of experimentation in preparation for the return of humans to the Moon, hopefully in the near future.

ACKNOWLEDGMENTS

We thank Allan D. Patchen for his assistance in the lab, particularly with electron microprobe analyses, and John Dunlap for his help with the TEM. We also thank the careful and thoughtful reviews by Rhian Jones and Sarah Noble. This work was partially supported by a NASA contract for dust mitigation studies to L.A.T., for which we are grateful. Additional funding was provided by the Planetary Geosciences Institute. Work of J.R.T. at ORNL was supported by DOE Office of Basic Energy Sciences, DMSandE. The Oak Ridge National Laboratory is managed by UT-Battelle, LLC for the United States Department of Energy under contract no. DE-AC05-00OR22725.

REFERENCES CITED

Allen, C.C., Lauer, H.V., Jr., Morris, R.V., and McKay, D.S. (1993) Microscopic iron metal on glass and minerals—a tool for studying regolith maturity. Icarus, 104, 291–300.

Allen, C.C., Morris, R.V., and McKay, D.S. (1996) An experimental analog to maturing lunar soil. Lunar Planetary Science, XXVII, 13–14.
Brecher, A., Menke, W.H., and Morash, K.R. (1974) Comparative magnetic studies of some Apollo 17 rocks and soils and their implications. Proceedings of the Fifth Lunar Science Conference, 3, 2795–2814.
Butler, R.F. (1992) Paleomagnetism: magnetic domains to geologic terranes, 336 p. Blackwell Scientific Publications, Oxford.
Dunlop, D.J. and Özdemir, O. (1997) Rock magnetism**:** fundamentals and frontiers, 573 p. Cambridge University Press, New York.
Ennas, G., Musinu, A., Piccaluga, G., Zedda, D., Gatteschi, D., Sangregorio, C., Stanger, J.L., Concas, G., and Spano, G. (1998) Characterization of iron oxide nanoparticles in an Fe_2O_3-SiO_2 composite prepared by a sol-gel method. Chemistry of Materials, 10, 495–502.
Hill, E. and Taylor, L.A. (2006) A reaction of lunar soil in a kitchen microwave oven. Geological Society of America Abstracts with Programs, 38, 68.
Hill, E., Mellin, M.J., Deane, B., Liu, Y., and Taylor, L.A. (2007) Apollo sample 70051 and high- and low-Ti lunar soil simulants MLS-1A and JSC-1A: Implications for future lunar exploration. Journal of Geophysical Research, 112, E02006, DOI: 10.1029/2006JE002767.
Keller, L.P. and McKay, D.S. (1997) The nature and origin of rims on lunar soil grains. Geochimica et Cosmochimica Acta, 61, 2331–2341.
McKay, D.S., Heiken, G.H., Basu, A., Blanford, G., Simon, S., Reedy, R., French, B.M., and Papike, J. (1991). The lunar regolith. In G.H. Heiken, D.T. Vaniman, B.M. French, Eds., Lunar Sourcebook: a User's Guide to the Moon, p. 285–356. Cambridge University Press, New York.
McKay, D.S., Carter, J.L., Boles, W.W., Allen, C.C., Allton, J.H. (1994). JSC-1: a new lunar soil simulant. Space IV, ASCE, 857–866.
Morris, R.V., Agresti, D.G., Lauer, H.V., Newcomb, J.A., Shelfer, T.D., and Murali, A.V. (1989) Evidence for pigmentary hematite on Mars based on optical, magnetic, and Mossbauer studies of superparamagnetic (nanocrystalline) hematite. Journal of Geophysical Research-Solid Earth and Planets, 94(B3), 2760–2778.
Morris, C.A., Anderson, M.L., Stroud, R.M., Merzbacher, C.I., and Rolison, D.R. (1999) Silica sol as a nanoglue: flexible synthesis of composite aerogels. Science, 284, 622–624.
Nagata, T., Fisher, R.M., Schwerer, F.C., Fuller, M.D., and Dunn, J.R. (1970) Magnetic properties and natural remanent magnetization of lunar materials. Proceedings of the Apollo 11 Lunar Science Conference, 3, 2325–2340.
——— (1972) Rock magnetism of Apollo 14 and 15 materials. Proceedings of the Third Lunar Science Conference, 3, 2423–2447.
——— (1973) Magnetic properties and natural remanant magnetization of Apollo 15 and 16 lunar materials. Proceedings of the Fourth Lunar Science Conference, 3, 3019–3043.
Nagata, T., Sugiura, N., Fisher, R.M., Schwerer, F.C., Fuller, M.D., and Dunn, J.R. (1974) Magnetic properties of Apollo 11–17 lunar materials with special reference to effects of meteorite impact. Proceedings of the Fifth Lunar Science Conference, 3, 2827–2839.
Noble, S.K., Pieters, C.M., and Keller, L.P. (2003) The optical properties of nanophase iron: investigation of a space weathering analog. In Lunar and Planetary Science XXXIV, Abstract 1172, Lunar and Planetary Institute, Houston (CD-ROM).
Park, J., Liu, Y., Khim, K.D., and Taylor, L.A. (2007) Characterizations of lunar dust due to health effect: particle size distribution and surface morphologies. Journal of Aeronautical Engineering, in press.
Pearce, G.W. and Chou, C.-L. (1977) On the origin of sample 70019 and its suitability for lunar magnetic field intensity studies. Proceedings of Lunar Science Conference, 8, 669–667.
Pearce, G.W., Gose, W.A., and Strangway, D.W. (1973) Magnetic studies of Apollo 15 and 16 lunar samples. Proceedings of the Fourth Lunar Science Conference, 3, 3045–3076.
Pearce, G.W., Strangway, D.W., and Gose, W.A., (1974) Magnetic properties of Apollo samples and implication for regolith formation. Proceedings of the Fifth Lunar Science Conference, 3, 2815–2826.
Sasaki, S., Nakamura, K., Hamabe, Y., Kurahashi, E., and Hiroi, T. (2001) Production of iron nanoparticles by laser irradiation in a simulation of lunar-like space weathering. Nature, 410, 555–557.
Shi, P. (1992) Fluid fugacities and phase equilibria in the Fe-Si-O-H-S system. American Mineralogist, 77, 1050–1066.
Taylor, L.A. (1992) Resources for a lunar base: rocks, minerals and soils of the Moon. In the second Conference on Lunar Base and Space Activities of the 21st Cenury. NASA Publ. 2, 361–377.
Taylor, L.A. and Meek, T.T. (2004) Microwave processing of lunar soil. In Proceedings of the International Lunar Conf. 2003/ILEWG5, American Astronautical Society 108 (Sciences and Technology Series), 109–123.
——— (2005) Microwave sintering of lunar soil: properties, theory, and practice. Journal of Aerospace Engineering, 18, 188–196.
Taylor, L.A., Pieters, C.M., Keller, L.P., Morris, R.V., and McKay, D.S. (2001) Lunar mare soils: space weathering and the major effects of surface-correlated nanophase Fe. Journal of Geophysical Research, 106 (11), 27,985–27,999.
Taylor, L.A., Schmitt, H.H., Carrier, W.D., and Nakagawa, M. (2005) The lunar dust problem: from liability to asset. 1st Space Explor. Conf., AIAA.
Wentworth, S.J., Keller, L.P., McKay, D.S., and Morris, R.V. (1999) Space weathering on the Moon: Patina on Apollo 17 samples 75075 and 76015. Meteoritics and Planetary Science, 34, 593–603.
Yamada, M., Sasaki, S., Nagahara, H., Fujiwara, A., Hasegawa, S., Yano, H., Hiroi, T., Ohashi, H., and Otake, H. (1999) Simulation of space weathering of planet-forming materials: Nanosecond pulse laser irradiation and proton implantation on olivine and pyroxene samples. Earth Planets and Space, 51, 1255–1265.

Manuscript received May 29, 2006
Manuscript accepted March 6, 2007
Manuscript handled by Rhian Jones